fluids

MDPI

Article

Thermal Hydraulics and Thermochemical Design of Fatty Acid Methyl Ester (Biodiesel) Esterification Reactor by Heating with High Boiling Point Phenyl-Naphthalene Liquid

Alon Davidy

Tomer Ltd., Tel-Aviv 6473424, Israel; alon.davidy@gmail.com; Tel.: +972-03-9049118

Abstract: FAME (biodiesel) is an alternative fuel that can be produced from vegetable oils. There is growing interest in the research and development of renewable energy sources. A possible solution is a biofuel usable in compression-ignition engines (diesel engines) produced from biomass rich in fats and oils. This paper contains a new and safer design of an esterification reactor for producing FAME (biodiesel) by utilizing high boiling point fluid (called phenyl-naphthalene). CFD simulation of biodiesel production by using methyl imidazolium hydrogen sulfate ionic liquid has been carried out. Ionic liquids (ILs) are composed of anions and cations that exist as liquids at relatively low temperatures. They have many advantages, such as chemical and thermal stability, low flammability, and low vapor pressures. In this work, the ionic liquids have been applied in organic reactions as solvents and catalysts of the esterification reaction. The great qualities of high boiling temperature fluids, along with advances in the oil and gas industries, make the organic concept more suitable and safer (water coming into contact with liquid metal may cause a steam explosion hazard) for heating the esterification reactor. The COMSOL Multiphysics code has been employed and simultaneously solves the continuity, fluid flow, heat transfer, and diffusion with chemical reaction kinetics equations. It was shown that the heat flux could provide the necessary heat flux required for maintaining the esterification process. It was found that the mass fractions of methanol and oleic acid decrease along the reactor axis. The FAME mass fraction increased along the reactor axis. The maximal biodiesel yield obtained in the esterification reactor was 86%. This value is very similar to the experimental results obtained by Elsheikh et al.

Keywords: biofuel; biodiesel production; CFD; methyl imidazolium hydrogen sulfate; ionic liquid; COMSOL Multiphysics; energy equation; diffusion equation with chemical reaction; high boiling fluid; phenyl-naphthalene

Citation: Davidy, A. Thermal Hydraulics and Thermochemical Design of Fatty Acid Methyl Ester (Biodiesel) Esterification Reactor by Heating with High Boiling Point Phenyl-Naphthalene Liquid. *Fluids* **2022**, *7*, 93. https://doi.org/10.3390/fluids7030093

Academic Editor: Marta María Mato Corzón

Received: 8 January 2022
Accepted: 2 March 2022
Published: 4 March 2022

1. Introduction

Ionic liquids (ILs) contain anions and cations that exist as liquids at relatively low temperatures. They have many advantages, such as chemical and thermal stability, low flammability, and low vapor pressures [1]. Because of these advantages, ionic liquids have been applied in organic reactions as solvents, catalysts, and liquid thermal storage fluids [2,3]. Ionic liquids are expensive. However, their higher cost may be easily manageable. This is because ionic liquids can be easily recycled back because of their low vapor pressure [4]. Extraction with solvents, adsorption, and separation by applying membranes may be used in order to separate the ionic liquid [5,6].

1.1. Review of the Biodiesel Production by Applying Ionic Liquid

The application of ionic liquids in biodiesel production has attracted the scientific community. It should be noted that employing ionic liquid may overcome several issues related to the traditional processes of biodiesel synthesis, such as employing homogenous alkaline catalysts, including NaOH and KOH, which make it compulsory to separate the

spent catalyst from fatty acid methyl ester (FAME) and the glycerol phase by additional washing steps [7]. However, this method has serious drawbacks, such as equipment caustic corrosion [8]. The production of biodiesel by using ionic liquid has several advantages. In biodiesel production, ionic liquids may reduce the number of reactions. They may decrease the energy consumption throughout the process. Most of the studies focus on the application of Brønsted acidic ionic liquids to biodiesel production [4]. Several studies regarding employing ionic liquids as catalysts for biodiesel production have been carried out. The first report using ionic liquids for biodiesel production has been published by the authors of Ref. [9]. They studied the methanolysis of several biodiesel production soybean oils with immobilized Candida antarctica lipase with various ionic liquids. It has been found that the production yield is eight times higher compared to a conventional solvent-free system and about 15% higher than using t -butanol as a solvent. The highest production of fatty acid methyl ester (FAME) has been obtained in commercially available 1-ethyl-3-methylimidazolium triflate. A patent dealing with the use of IL as solvents for biodiesel production has been submitted by the authors of Ref. [10]. Elsheikh et al. [11] performed experiments using an imidazolium ring. It was found that the best catalyst was 1-butyl-3-methylimidazolium hydrogen sulfate [BMIM][HSO_4]. They achieved 91.2% conversion. The reaction temperature was 160 °C, and the reaction time was 2 h. Fauzi and Amin [12] carried out multi-objective optimization for the esterification reaction between methanol and oleic acid catalyzed by ionic liquid 1-butyl-3-methylimidazolium hydrogen sulfate [BMIM][HSO_4]. They applied an artificial neural network genetic algorithm in order to optimize the main variables: the molar ratio between methanol and oleic acid, temperature, reaction time, and catalyst dosage. They found that the optimal parameters are: temperature of 87 °C and reaction time of 5.2 h. The conversion of oleic acid is 80.4%.

Numerical Simulations of Biodiesel Production

Computational fluid dynamics simulations of biodiesel production have been carried out by applying the eddy dissipation model (EDM) coupled with the Reynolds stress model (RSM). The calculated biodiesel yield compared well with the experimental results [13]. Mekala applied ANSYS Fluent code in order to solve fluid flow, heat, and mass transfer transport equations in packed beds reactors [14]. This work contains a Multiphysics design of an esterification reactor for the transformation of oleic acid and methanol to FAME by employing high boiling point fluid. As far as I know, it is the first time that phenyl-naphthalene has been proposed to supply the required heat needed to sustain the esterification reaction for FAME.

1.2. Advantages of Applying High Boiling Liquid Heat Carriers

High temperature heat carriers have been employed for high temperature heating. The main advantages of these heat carriers are [15,16]:

(1) By using high boiling point liquids operating at atmospheric pressure, it is possible to construct heating plants that are very easy to run and are reliable in operation.
(2) It is possible to control the heating temperature.
(3) The great qualities of high boiling temperature liquids make them more suitable and safer. This is because water coming into contact with liquid metal may cause a steam explosion hazard.
(4) It eliminates the need of using heavy forgings for pressure vessels and piping.
(5) Heat carrier compatibility with low-cost materials and virtually no corrosion potential enables the usage of plain carbon steel and aluminum alloys.

Critical Heat Flux of Water

There are several advantages of using two-phase heating. A poorly designed two-phase heating system may fail due to critical heat flux. Figure 1 shows the typical boiling curve of water [17].

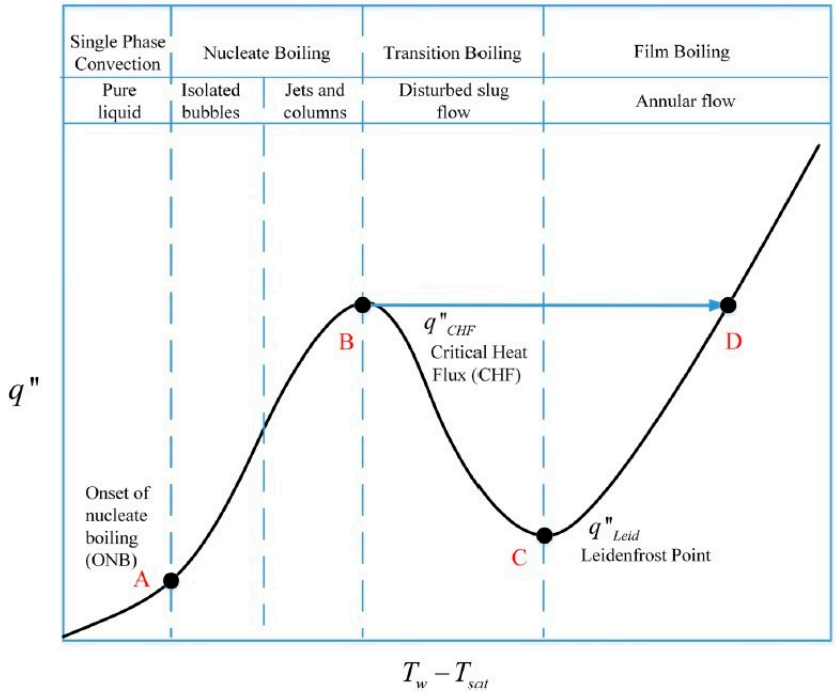

Figure 1. Boiling curve of water (Reprinted from Ref. [17]).

This curve can be divided into four segments. In the first segment, at low temperature drops, the line OA is straight. In this segment, the heat is transferred by single phase convection up to point B, where bubbles are produced on the wall surface. The second segment, line AB, is also approximately straight, but its slope is greater than that of line OA.

From point B to C, there is a nucleate boiling region. In this regime, bubbles are generated at fixed nucleation sites on the wall. At higher heat fluxes, the number of nucleation sites increases. Bubbles from the same sites coalesce and eventually form irregular columns of vapor leaving the surface [18]. The second segment terminates at the point of maximum flux, which is point B in Figure 1. The heat flux at point B is called critical heat flux (CHF). At the point of dry-out, the depletion of the liquid layer leads to a significant decrease in the heat transfer at the surface, which will result in a decrease in the wall temperature. At this point, the rapid nucleation of bubbles results in the formation of dry areas, which cover large surface areas. A vapor film separates the liquid from the surface, and the film boiling has been initiated. This causes a drastic reduction in heat transfer from the fluid to the esterification reactor walls since the vapor has a much lower thermal conductivity than the liquid. This condition is referred to as a departure from nucleate boiling (DNB), where the point of maximum heat flux is called the critical heat flux (CHF). Phenyl-naphthalene exhibits a better heat transfer performance. It does not boil at 160 °C like water. In the third segment, line BC in Figure 1, the flux decreases as the temperature drop rises and reached a minimum at point C. Point C is called the Leidenfrost point. This point is referred to as the minimum heat flux, second boiling crisis. In the last segment, line CD, the flux again increases with the ΔT [19] (natural convection curve).

2. Materials and Methods

2.1. Thermophysical Properties of Methylimidazolium Hydrogen Sulfate

The thermo-physical properties of the imidazolium salt are shown in Table 1 [20,21].

Table 1. Thermo-physical properties of imidazolium salt (Data from Refs. [20,21]).

Material Property	Value
ρ	1367 (kg/m^3)
Cp	1280 (J/(kg·°C))
k	0.2 (w/(m·°C))
η	0.0367 (Pa·s)

2.2. Multiphysics Analyses of the Esterification Reactor

The numerical analysis of the FAME reactor is described in this subsection. Figure 2 shows the schematic of the proposed esterification reactor of oleic acid and methanol to FAME.

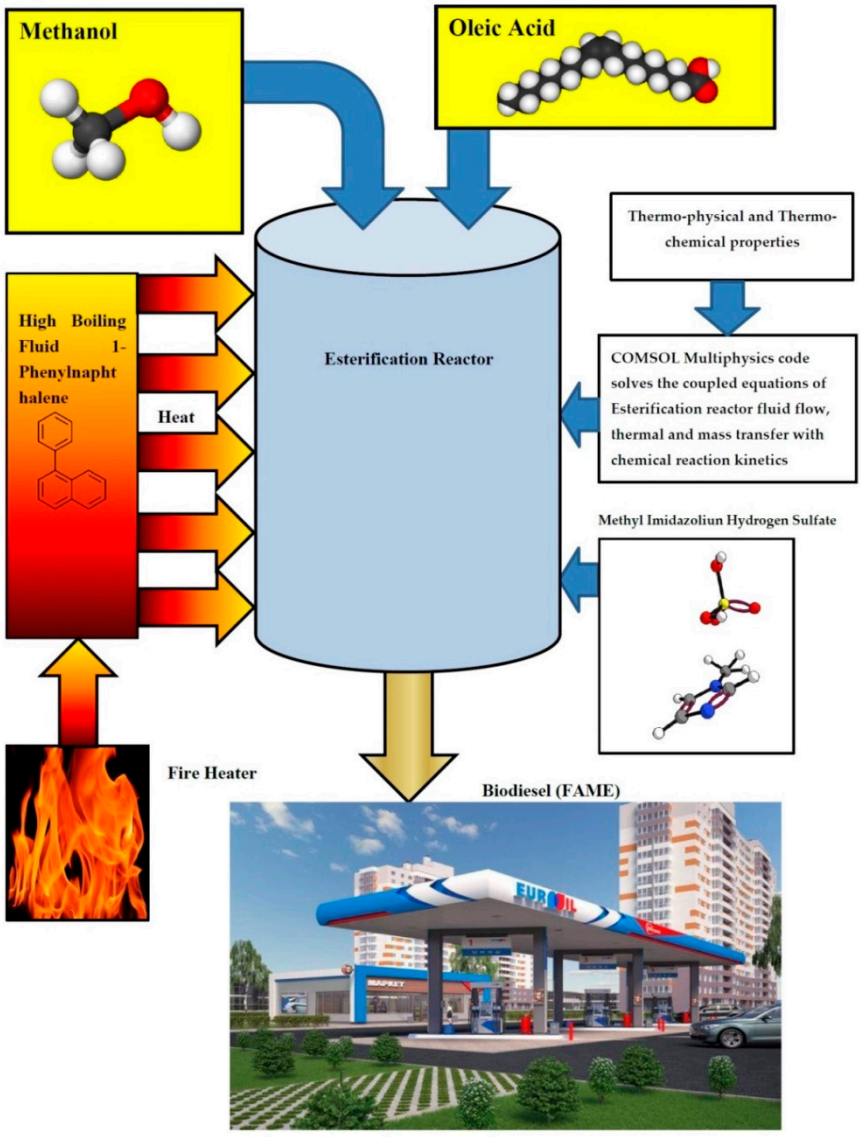

Figure 2. Schematics of the proposed esterification reactor of oleic acid and methanol to FAME.

As can be seen from Figure 2, the phenyl-naphthalene liquid is heated by the fire heater. COMSOL Multiphysics software has been applied in this research and solved simultaneously the transient transport equations mass conservation (continuity), fluid flow (Navier–Stokes), energy, and diffusion with esterification reaction equations. Section 2.2.1 describes in detail the esterification reaction kinetics. Section 2.2.2 describes the continuity

and fluid flow. Sections 2.2.3 and 2.2.4 describe the energy transport and diffusion equations. The geometry of this reactor is shown in Figure 3.

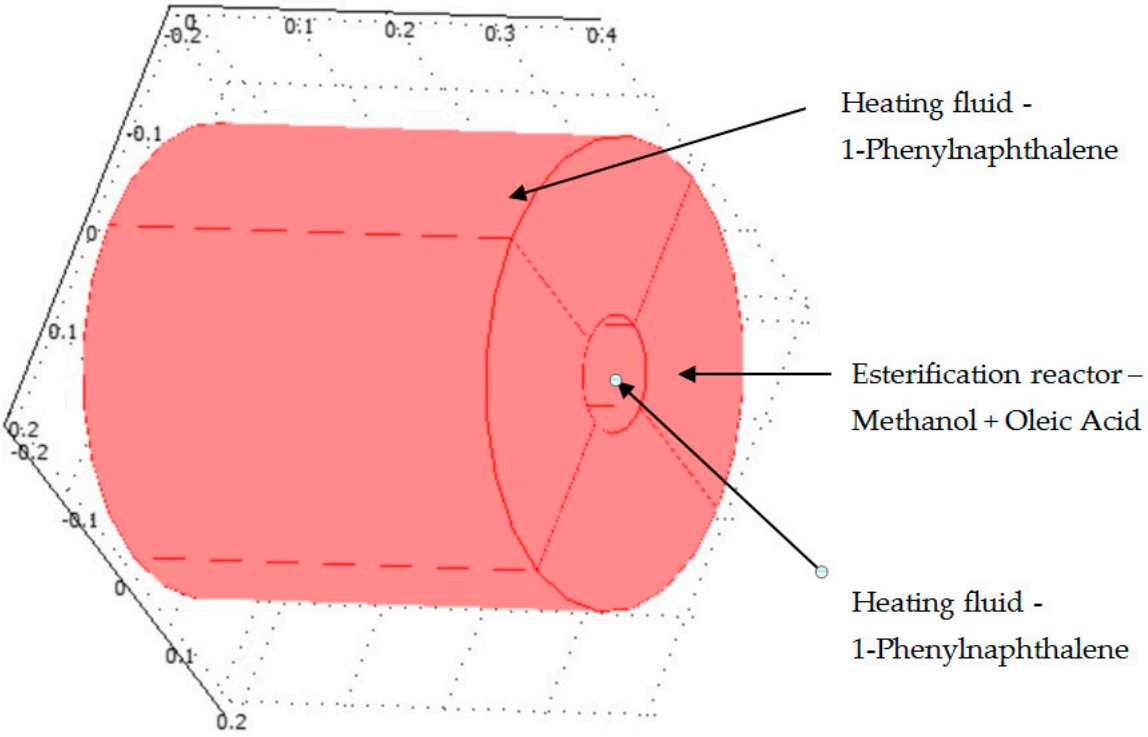

Figure 3. 3D plot of esterification reactor.

The height of the esterification reactor is 0.4 m, and its radius is 0.05 m. The esterification chemical reaction occurred inside the reactor. The heat is supplied at the inner and outer radius of the reactor. Methanol and oleic acid have been mixed in stoichiometric amounts inside the reactor. This model studies the esterification of oleic acid and methanol into FAME.

2.2.1. Model Kinetics

Inside the esterification reactor, oleic acid and methanol react together to form FAME and water [4]:

$$C_{18}H_{34}O_2 + CH_3OH \rightarrow C_{19}H_{36}O_2 + H_2O \quad (1)$$

The esterification reaction rate is calculated according to [4]:

$$k = A \exp\left(-\frac{E}{RT}\right) \quad (2)$$

The value of frequency factor, A, is 1.083×10^{10} (1/s) [22]. The value of the activation energy, E, is 84,384 (J/mole) [22]. This reaction consumes heat from the phenyl-naphthalene (endothermic reaction). The FAME production rate in (mole/(m^3·s)) is given by:

$$R_{FAME} = kc_{OA}c_{Met} \quad (3)$$

The Arrhenius plot of the oleic acid conversion to FAME (biodiesel) is shown in Figure 4.

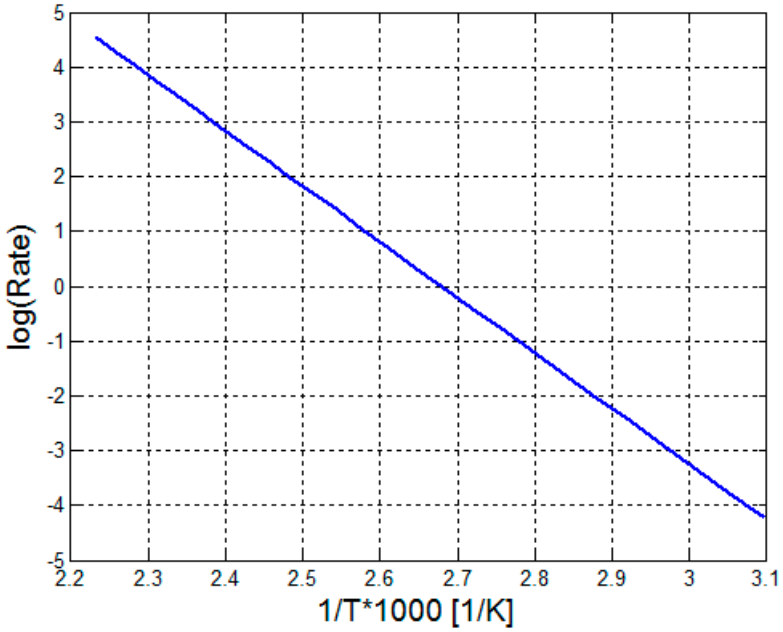

Figure 4. Arrhenius plot of the oleic acid and methanol conversion to FAME (biodiesel) and water.

Figure 4 shows that the esterification reaction rate increases with the temperature. At 160 °C (0.0023 1/K), the reaction rate is about 55 [1/min].

2.2.2. Fluid Flow and Continuity Equations

Since the esterification reaction is slow, it is assumed that the flow of reactants and products inside the esterification reactor is laminar. The flow of species is described by applying steady state Navier–Stokes equation [23]:

$$\rho \partial \mathbf{u}/\partial t - \nabla \cdot \eta\left(\nabla \mathbf{u} + (\nabla \mathbf{u})^T\right) + \rho \mathbf{u} \cdot \nabla \mathbf{u} + \nabla p = \mathbf{F} \quad (4)$$

Here, **F** is a body force (gravity) term (N/m^3). Since the flow is incompressible, the mass conservation equation for the reacting species is [23]:

$$\nabla \cdot \mathbf{u} = 0 \quad (5)$$

2.2.3. Heat Transfer Equation

The heat transfer equation applied to the esterification reactor considers forced convection, conduction, and heat loss by endothermic reaction [23]:

$$\rho c_p(\partial T/\partial t + \mathbf{u} \cdot \nabla T) - \nabla \cdot (-k \nabla T) = Q \quad (6)$$

Q is the heat density of esterification term (W/m^3). It is calculated by the following equation:

$$Q = R_{FAME} \cdot \Delta H \quad (7)$$

where ΔH is the heat of the esterification reaction in (J/mole). The enthalpy of esterification reaction has been calculated according to the following equation:

$$\Delta H = H_{f,FAME} + H_{f,H_2O} - H_{f,CH_3OH} - H_{f,OA}$$

The formation enthalpies of the reactants and the products have been taken from Refs. [24,25]. The calculated heat of the esterification reaction is: 158.7 J/mole.

2.2.4. Diffusion Transport Equation

The mass transfer in the esterification reactor contains convection, diffusion, and chemical reaction terms. The transient diffusion equation for oleic acid (OA) is provided in Equation (8):

$$\partial c_{OA}/\partial t + \nabla \cdot (-D_{OA}\nabla c_{OA} + c_{OA}\mathbf{u}) = -R_{OA} \quad (8)$$

The transient diffusion equation of the methanol is provided in the following Equation (9):

$$\partial c_{Met}/\partial t + \nabla \cdot (-D_{Met}\nabla c_{Met} + c_{Met}\mathbf{u}) = -R_{Met} \quad (9)$$

The diffusion equation for the FAME is provided in Equation (10):

$$\partial c_{FAME}/\partial t + \nabla \cdot (-D_{FAME}\nabla c_{FAME} + c_{FAME}\mathbf{u}) = R_{FAME} \quad (10)$$

The conversion of OA is calculated according to Equation (11).

$$X_{OA} = \frac{c_{OA,in} - c_{OA,out}}{c_{OA,in}} \quad (11)$$

2.3. Thermo-Physical Properties of 1-Phenylnaphthalene

The thermo-physical properties of the 1-phenylnaphthalene are provided in Table 2 [26].

Table 2. Thermo-physical properties of 1-phenylnaphthalene (Data from Ref. [26]).

Material Property	Value
ρ	358 (kg/m^3)
Cp	2323 (J/(kg·°C))
k	0.077 (W/(m·°C))
η	0.00011 (Pa·s)

2.4. Calculation of Convective Heat Transfer Inside the Reactor Hole

It is assumed that the 1-phenylnaphthalene fluid flows inside the internal hole of the reactor. Dittus–Bolter empirical equation has been applied in order to calculate the convective coefficient of the hot stream [27].

$$Nu = 0.023\mathrm{Re}^{0.8}\mathrm{Pr}^{0.4} \quad (12)$$

The Reynolds number (Re) is the ratio of inertial forces to viscous forces. It is calculated by the following equation [27]:

$$\mathrm{Re} = \frac{vD\rho_p}{\eta_p} \quad (13)$$

The Prandtl number (Pr) is the ratio of momentum diffusivity to thermal diffusivity of the high boiling point liquid. It is calculated by the following equation [27]:

$$\mathrm{Pr} = \frac{\eta_p k_p}{c_{p_p}} \quad (14)$$

The convective heat transfer coefficient, h, is obtained by using Equation (11):

$$h = 80\frac{\mathrm{w}}{\mathrm{m}\cdot\mathrm{K}} \quad (15)$$

The convective heat transfer coefficient of the water vapor at temperature of 160 °C and at atmospheric pressure has been calculated by applying the Dittus–Boelter empirical equation (Equation (12)). The convective heat transfer coefficient obtained for water vapor is 2.3 W/(m·K). Thus, phenyl-naphthalene is a superior heating medium.

2.5. Boundary Conditions

It is assumed that concentrations of methanol and oleic acid entering the esterification reactor are 100 mol/m^3, respectively. Thus, the boundary conditions applied to solve the diffusion equations for the methanol and oleic acid are:

$$c_{Met}|_{z=0} = c_{OA}|_{z=0} = 100 \text{ mol/m}^3 \text{ ; } c_{FAME}|_{z=0} = 0.1 \text{ mol/m}^3 \quad (16)$$

It is assumed that the reactor walls are impermeable to the methanol, oleic acid, and *FAME*.

$$-n(-D\nabla c_{Met})|_{r=r_{in}} = -n(-D\nabla c_{OA})|_{r=r_{in}} = -n(-D\nabla c_{FAME})|_{r=r_{in}} = 0 \quad (17)$$

$$-n(-D\nabla c_{Met})|_{r=r_{out}} = -n(-D\nabla c_{OA})|_{r=r_{out}} = -n(-D\nabla c_{FAME})|_{r=r_{out}} = 0 \quad (18)$$

Convective mass flux at the reactor outlet:

$$-n(-D\nabla c_{Met})|_{z=h} = -n(-D\nabla c_{OA})|_{z=h} = -n(-D\nabla c_{FAME})|_{z=h} = 0 \quad (19)$$

It is assumed that temperature of methanol and oleic acid entering the esterification reactor is 160 °C. The boundary conditions required to solve the heat transfer equations are:

$$T|_{z=0} = 160\ ^{\circ}\text{C} \quad (20)$$

$$-n(-k\nabla T)|_{r=r_{in}} = h(160 - T) \quad (21)$$

$$-n(-k\nabla T)|_{r=r_{out}} = h(160 - T) \quad (22)$$

Convective heat flux at the reactor outlet:

$$-n(-k\nabla T)|_{z=h} = 0 \quad (23)$$

The boundary conditions required to solve the flow equations are:

$$v|_{z=0} = 3 \text{ mm/s ; } u|_{z=0} = w|_{z=0} = 0 \quad (24)$$

Non-slip conditions at the reactor inner and outer walls:

$$u|_{r=r_{in}} = w|_{r=r_{in}} = v|_{r=r_{in}} = 0 \quad (25)$$

$$u|_{r=r_{out}} = w|_{r=r_{out}} = v|_{r=r_{out}} = 0 \quad (26)$$

The pressure at the reactor outlet is equal to atmospheric pressure:

$$p|_{z=h} = p_{atm} \quad (27)$$

3. Results

This section shows the numerical results for the concentration and temperature fields inside the esterification reactor.

Numerical Model Convergence and Validation

It was assumed that the temperature of the oleic acid and methanol entering the esterification reactor was 160 °C. In order to avoid the boiling and evaporation of the water generated during the esterification reaction, the pressure inside the esterification reactor was 700 kPa. It should be noted that the saturated pressure of water at T = 160 °C is 620 kPa [28]. Since the water droplets generated during the esterification reaction are heavier than the gas, they fall and are extracted from the reactor bottom. They may react with ionic liquid, mostly at the reactor inlet. Moreover, if the heating system fails (due to an electric power supply failure or technical problem inside the phenyl-naphthalene liquid

pump), the steam may condensate inside the esterification reactor, leading to the generation of water bubbles and decreasing further the heat transfer to the esterification reactor. Thus, it may be difficult to resume the normal operation of the esterification reactor. By applying high pressure, it is easier to resume the operation of this reactor. In some cases, there are side reactions between water and ionic liquids [29]. To combat this problem, the water is removed. Figure 5 shows the convergence plot.

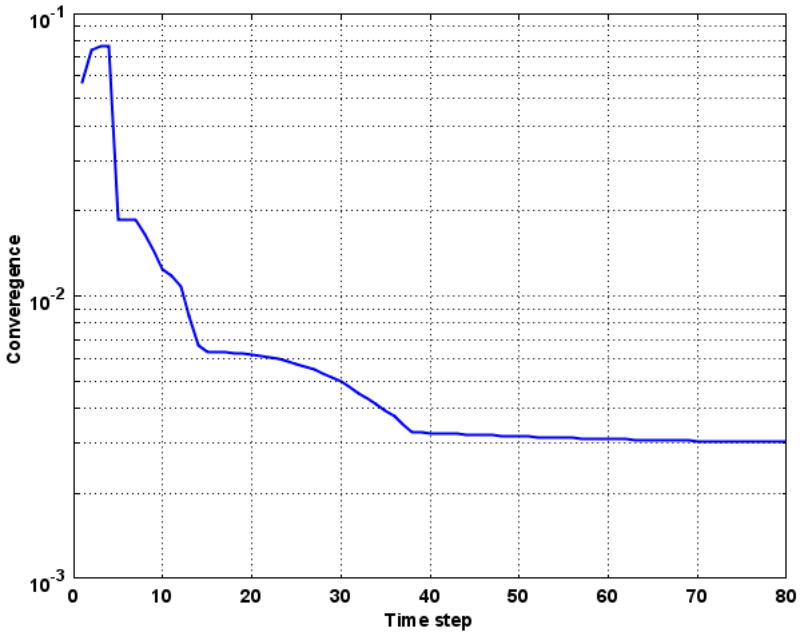

Figure 5. Convergence plot.

Figure 5 shows that the numerical results of the concentration, velocity, and temperature have been converged. The convergence has been decreased by 96% (from 0.08 to 0.003). Figure 6 shows the error plot.

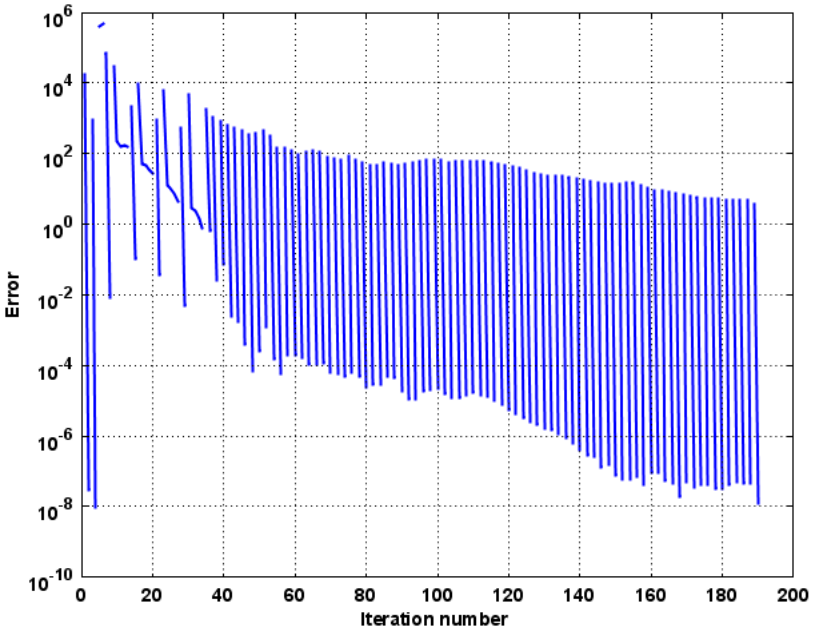

Figure 6. Error plot.

Figure 6 shows that the numerical errors of the concentration, velocity, and temperature have been decreased by 12 magnitudes (from 1×10^4 to 1×10^{-8}). The maximal

biodiesel yield obtained in the esterification reactor is 86% after 7200 s (2 h). This value is very similar to the experimental results obtained by Elsheikh et al. [11]. He performed experiments using an imidazolium ring. It was found that the best catalyst is 1-butyl-3-methylimidazolium hydrogen sulfate [BMIM][HSO_4]. He achieved 91.2% conversion. The reaction temperature was 160 °C, and the reaction time was 2 h. Figure 7 shows the three-dimensional temperature field inside the esterification reactor at t = 20,000 s.

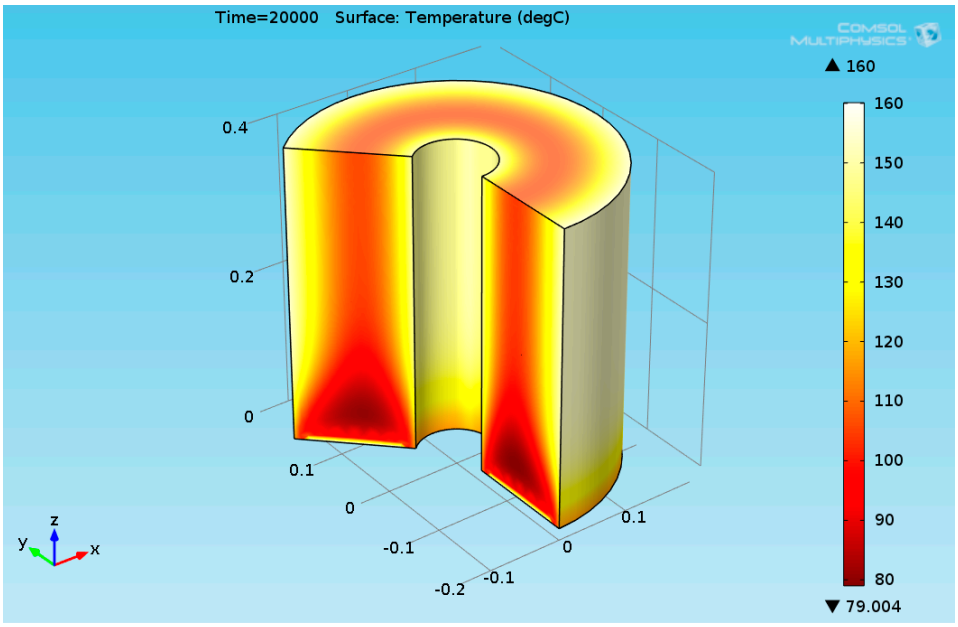

Figure 7. 3D plot of the temperature field inside the esterification reactor at t = 20,000 s.

It can be seen from Figure 7 that the temperature at the lower section of the reactor is higher than the temperature at the upper side. This is because the endothermic esterification reaction consumes the heat provided by the phenyl-naphthalene liquid. It should be noted that the thermal conductivity of the ionic liquid and reactants (oleic acid and methanol) has a lower value. Figure 8 shows the 3D FAME concentration field inside the reactor.

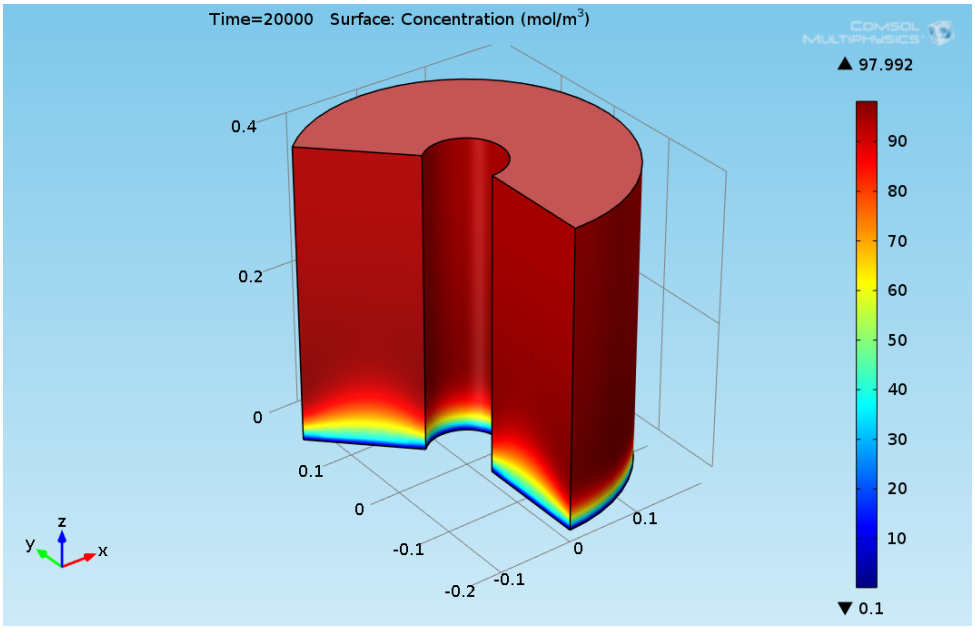

Figure 8. 3D plot of the concentration field of the FAME inside the esterification reactor.

Figure 8 shows that the FAME conversion is about 100%. A similar value has been obtained in Ref. [4] for T = 130 °C and 5.6 h. Figure 9 shows the 3D oleic acid concentration field inside the reactor.

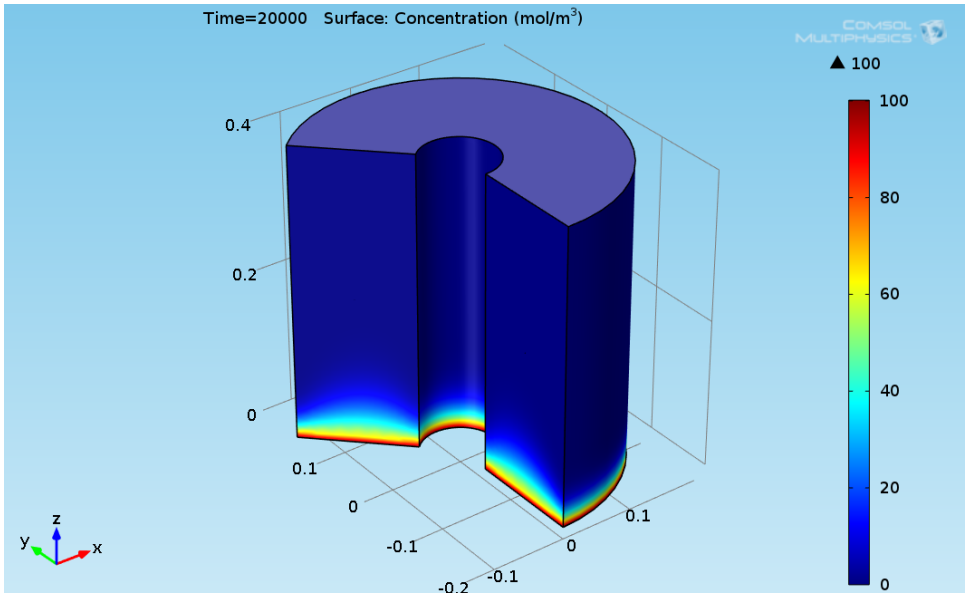

Figure 9. 3D plot of the concentration field of the oleic acid inside the esterification reactor.

Figure 9 indicates that the oleic acid and methanol transformed almost completely to FAME (biodiesel) and water at t = 20,000 s. Figure 10 shows the axial FAME concentration along the reactor height.

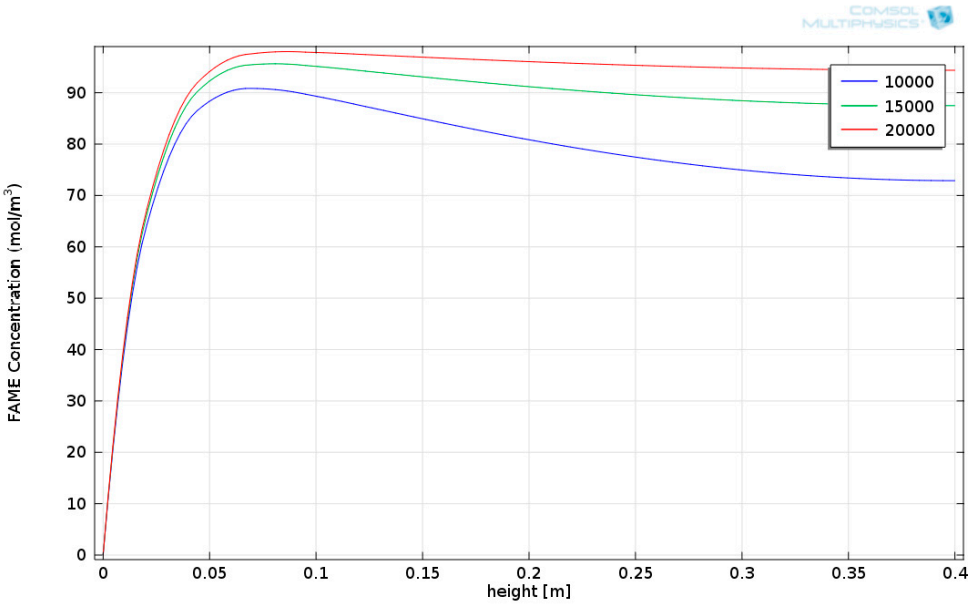

Figure 10. Axial plot of the FAME concentration along the esterification reactor height for phenylnaphthalene liquid at temperature of 160 °C.

Figure 10 shows that the FAME concentration increases with time. There is a slight decrease in FAME from y = 0.1 m until y = 0.4 m. This is because the thermal conductivities of the ionic liquid and reactants (oleic acid and methanol) have lower values. Figure 11 shows the axial FAME concentration along the reactor height at T = 50 °C.

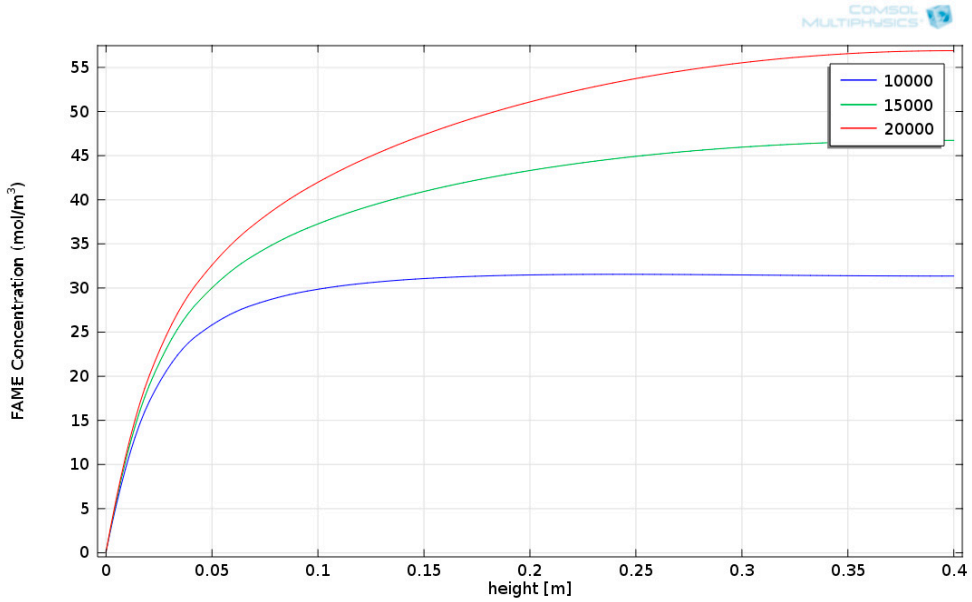

Figure 11. Axial plot of the FAME concentration along the esterification reactor height for phenyl-naphthalene liquid at temperature of 50 °C.

Figure 11 shows that the FAME yield has lower values for phenyl-naphthalene liquid at a temperature of 50 °C.

4. Discussion

The convective heat transfer coefficient of the water vapor at a temperature of 160 °C and an atmospheric pressure has been calculated by applying the Dittus–Boelter empirical equation. The convective heat transfer coefficient obtained for water vapor is 2.3 W/(m·K). The convective heat transfer coefficient obtained for phenyl-naphthalene at the same conditions is 80 W/(m·K). Thus, phenyl-naphthalene is a superior heating medium.

The maximal biodiesel yield obtained in the esterification reactor is 86% at t = 7200 s (2 h). This value is very similar to the experimental results obtained by previous works. This work shows that the oleic acid and methanol transformed almost completely to FAME (biodiesel) and water at t = 15,000 s (about 4.2 h) and t = 20,000 s. The FAME yield obtained in this work is close to 95% for T = 160 ° with a reaction time of 4.2 h. Similar values have been obtained in Ref. [4] for T = 130 °C and 5.6 h. It has been found that the FAME concentration increases with time. There is a slight decrease in the FAME from y = 0.1 m until y = 0.4 m. However, for longer times (at t = 20,000 s), the FAME yield is nearly constant from h = 0.05 m until h = 0.4 m. This phenomenon is probably caused due to the decay of the heat transfer flux entering the esterification reactor. This is because the thermal conductivities of the ionic liquid and reactants (oleic acid and methanol) have lower values. It has been shown that the FAME yield has lower values for phenyl-naphthalene liquid at a temperature of 50 °C.

5. Conclusions

This paper presented an advanced CFD simulation of biodiesel production by applying imidazolium ionic liquid. COMSOL software simultaneously solves mass conservation (continuity), fluid flow (Navier–Stokes), heat transfer, and diffusion with esterification reaction transport equations. It has been shown that the heat flux can provide the required heat flux for maintaining the esterification process. It has been found that the concentrations of methanol and oleic acid decrease along the reactor axis. The FAME mass fraction increases along the esterification reactor axis. This is because the endothermic reactions consume the heat. The internal and external surfaces of the reactor are exposed to heat supplied by phenyl-naphthalene high boiling fluid. In order to avoid the boiling and

evaporation of the water generated inside the esterification reaction, the pressure inside the esterification reactor is set to 700 kPa. It should be noted that the saturated pressure of water at T = 160 °C is 620 kPa. Since the water droplets generated during the esterification reaction are heavier than the gas, they fall and are extracted from the bottom. They may react with ionic liquid, mostly at the reactor inlet. Moreover, if the heating system fails (due to an electric power supply failure or technical problem inside the phenyl-naphthalene liquid pump), the steam may condensate inside the esterification reactor, leading to the generation of water bubbles and decreasing further the heat transfer to the esterification reactor. Thus, it may be difficult to resume the normal operation of the esterification reactor. By applying high pressure, it is easier to resume the operation of this reactor. In some cases, there are side reactions between water and ionic liquids. To combat this problem, the water is removed. A petroleum coke burner can provide the necessary heat flux for the esterification reactor. It is possible to apply this reactor near the delayed coker unit (DCU) in order to produce diesel and biodiesel fuels.

Funding: This research has not received external funding.

Conflicts of Interest: The author declares no conflict of interest.

Nomenclature

A	frequency factor in [1/s]
C	concentration
c_p	specific heat in [J/(kg·K)]
D	diffusion coefficient in [m^2/s]
E	activation energy in [J/mole]
H_f	enthalpy of formation in [J/mole]
h	convective coefficient in [W/(m^2·K)]
k	thermal conductivity in [W/(m·K)]
p	pressure in [Pa]
p_{atm}	atmospheric pressure in [Pa]
Pr	Prandtl number
R	reaction rate on [mole/(m^3·s)]
$\overline{R}$	gas constant (8.3143 J/(mole·K))
Re	Reynolds number
r_{in}	inner radius [m]
r_{out}	outer radius [m]
Nu	Nusselt number
T	temperature in [K]
X	conversion
$\mathbf{u}(u, v, w)$	velocity vector in [m/s]
Subscripts	
FAME	fatty acid methyl ester
in	inlet, inner radius
Met	methanol
OA	oleic acid
Out	outlet, outer
P	phenylnaphthalene liquid
Greek letters	
η	viscosity in [Pa·s]
ν	velocity of Phenylnaphthalene liquid in [m/s]
ρ	density in [kg/m^3]
Abbreviation	
FAME	fatty acid methyl ester
IL	ionic liquid

References

1. Fang, Z.; Smith, R.L., Jr.; Qi, X. *Productions of Biofuels and Chemicals with Ionic Liquid*; Springer: Heidelberg, Germany, 2014.
2. Tran, A.T.; Tomlin, J.; Lam, P.H.; Stinger, B.L.; Miller, A.D.; Walczyk, D.J.; Cruz, O.; Vaden, T.D.; Yu, L. Conductivity, Viscosity, Spectroscopic Properties of Organic Sulfonic Acid solutions in Ionic Liquids. *ChemEngineering* **2019**, *3*, 81. Available online: https://www.mdpi.com/2305-7084/3/4/81 (accessed on 7 January 2022). [CrossRef]
3. Wu, B.; Reddy, R.G.; Rogers, R.D. Novel Ionic Liquid Thermal Storage for Solar Thermal Electric Power Systems. In Proceedings of the Solar Forum 2001, Solar Energy: The Power to Choose, Washington, DC, USA, 21–25 April 2001.
4. Roman, F.F. Biodiesel Production Through Esterification Applying Ionic Liquid as Catalyst. Master's Thesis, Escola Superior de Tecnologia e Gestão do Instituto Politécnico de Bragança, Braganca, Portugal, 2018.
5. Mai, N.L.; Ahn, K.; Koo, Y.-M. Methods for recovery of ionic liquids—A review. *Process Biochem.* **2014**, *49*, 872–881. [CrossRef]
6. Kuzmina, O.; Hallet, J.P. *Application Purification and Recovery of Ionic Liquid*; Elsevier: Amsterdam, The Netherlands, 2016.
7. Lucu, R.; Melero, J.A. *Advances in Biodiesel Production Processes and Technologies*; Woodhead Publishing Limited: Cambridge, UK, 2012.
8. Hamdy Makhlouf, A.S.; Aliofkhazraei, M. *Handbook of Material Failure Analysis with Case Studies from the Chemicals, Concrete and Power Industries*; Elsevier: Amsterdam, The Netherlands, 2016.
9. Ha, S.; Lan, M.; Lee, S.; Hwang, S.; Koo, Y. Lipase-catalyzed biodiesel production from soybean oil in ionic liquids. *Enzym. Microbiol. Technol.* **2007**, *41*, 480–483. [CrossRef]
10. Lozano, P.; De Tiego, T.; Iborra, J.; Vaultier, M. Use of Ionic Liquids for Implementing a Process for the Preparation of Biodiesel. European Patent EP 2189535 A1, 21 November 2008.
11. Elsheikh, Y.A.; Man, Z.; Bustam, M.A.; Yusup, S.; Wilfred, C.D. Brønsted imidazolium ionic liquids: Synthesis and comparison of their catalytic activities as pre-catalyst for biodiesel production through two stage process. *Energy Convers. Manag.* **2011**, *52*, 804–809. [CrossRef]
12. Fauzi, A.H.M.; Amin, N.A.S. Optimization of oleic acid esterification catalyzed by ionic liquid for green biodiesel synthesis. *Energy Convers. Manag.* **2013**, *76*, 818–827. [CrossRef]
13. Mohiuddin, A.K.M.; Adeyemi, N. Numerical Simulation of Biodiesel Production Using Waste Cooking Oil. In Proceedings of the ASME 2013 International Mechanical Engineering Congress and Exposition IMECE2013, San Diego, CA, USA, 15–21 November 2013.
14. Mekala, S.J. CFD Studies of Reactive Flow with Thermal and Mass Diffusional effects in a Supercritical Packed Bed Catalytic Reactor. Ph.D. Thesis, Universitat Politècnica de Catalunya, Barcelona, Spain, 2016.
15. Chechetkin, A.V. *High Temperature Heat Carriers, Pergamon Press Book*; The Macmillam Company: New Yok, NY, USA, 1963.
16. Shirvan, K.; Forest, E. Design of an Organic Simplified Nuclear Reactor. *Nucl. Eng. Technol.* **2016**, *48*, 893–905. [CrossRef]
17. Davidy, A. CFD Design of Hydrogenation Reactor for Transformation of Levulinic Acid to γ-Valerolactone (GVL) by using High Boiling Point Organic Fluids. *ChemEngineering* **2019**, *3*, 32. [CrossRef]
18. Hewitt, G.F. Chapter 7: Pool Boiling. In *Two Phase Flow and Heat Transfer*; Butterworth, D., Hewitt, G.F., Eds.; Oxford University Press: Oxford, UK, 1977.
19. McCabe, W.L.; Smith, J.C. *Unit Operations of Chemical Engineering*, 2nd ed.; MacGraw-Hill, Inc.: New York, NY, USA, 1967.
20. Marcus, Y. *Ionic Liquid Properties from molten salt to RTIL*; Springer International Publishing: Cham, Switzerland, 2016.
21. Zhao, H. Innovative Applications of ionic liquids as "green" engineering liquids. *Chem. Eng. Commun.* **2006**, *193*, 1660–1677. [CrossRef]
22. Li, J.; Guo, Z. Structure Evolution of Synthetic Amino Acids-Derived Basic Ionic Liquids for Catalytic Production of Biodiesel. *ACS Sustain. Chem. Eng.* **2017**, *5*, 1237–1247. [CrossRef]
23. COMSOL. *Multiphysics—Modeling Guide, Version 4.3b*; COMSOL AB: Stockholm, Sweden, 2013.
24. Cheméo, High Quality Chemical Properties Web Site. Available online: https://www.chemeo.com/ (accessed on 5 February 2022).
25. Standard Enthalpy of Formation. Available online: https://en.wikipedia.org/wiki/Standard_enthalpy_of_formation (accessed on 5 February 2022).
26. McFarlane, J.; Luo, H.; Garland, M.; Steele, W.V. Evaluation of Phenylnaphthalenes as Heat Transfer Fluids for High Temperature Energy Applications. *Sep. Sci. Technol.* **2010**, *45*, 1908–1920. [CrossRef]
27. Bergman, T.L.; Incropera, F.P.; DeWitt, D.P.; Lavine, A.S. *Fundamentals of Heat and Mass Transfer*; John Wiley & Sons: Hoboken, NJ, USA, 2011.
28. Moran, M.J.; Shapiro, H.N.; Boettner, D.D.; Bailey, M.B. *Fundamentals of Engineering Thermodynamics*, 7th ed.; John Wiley and Sons: Hoboken, NJ, USA, 2011.
29. Gräsvik, J. Ionic liquids in bio-Refining Synthesis and Applications. Ph.D. Thesis, Umeå University, Umea, Sweden, 2013.